nature materials

LETTERS

https://doi.org/10.1038/s41563-019-0508-z

Soft dendritic microparticles with unusual adhesion and structuring properties

Sangchul Roh[1], Austin H. Williams[1], Rachel S. Bang[1], Simeon D. Stoyanov[1,2,3,4] and Orlin D. Velev[1*]

The interplay between morphology, excluded volume and adhesivity of particles critically determines the physical properties of numerous soft materials and coatings[1–6]. Branched particles[2] or nanofibres[3], nanofibrillated cellulose[4] or fumed silica[5] can enhance the structure-building abilities of colloids, whose adhesion may also be increased by capillarity or binding agents[6]. Nonetheless, alternative mechanisms of strong adhesion found in nature involve fibrillar mats with numerous subcontacts (contact splitting)[7–11] as seen in the feet of gecko lizards and spider webs[12–17]. Here, we describe the fabrication of hierarchically structured polymeric microparticles having branched nanofibre coronas with a dendritic morphology. Polymer precipitation in highly turbulent flow results in microparticles with fractal branching and nanofibrillar contact splitting that exhibit gelation at very low volume fractions, strong interparticle adhesion and binding into coatings and non-woven sheets. These soft dendritic particles also have potential advantages for food, personal care or pharmaceutical product formulations.

The soft dendritic particles with colloidal-sized branches (dendricolloids) are fabricated by a simple and scalable process of polymer precipitation in turbulently sheared liquid medium (Fig. 1a). The polymer solution is injected into the non-solvent medium in high shear rate rotor–stator mixer (Methods and Supplementary Fig. 1). The interfacial tension between the polymer solution and the medium is ultralow because of their mutual miscibility[1,18,19]. As a result, the polymer solution is intensively sheared and dispersed. Concurrent polymer phase separation and precipitation result in the formation of dendritic fibrillar particles (Fig. 1a). The typical morphology of the soft material is illustrated in Fig. 1a–d and Supplementary Video 1. The dendricolloids are hierarchically branched and thus surrounded by a nanofibrillar corona spreading out in all directions. We first discuss the principles of the liquid shear precipitation method that enable the transformation of a wide variety of common polymers into soft dendritic material. We then analyse how the morphology of the soft dendritic microparticles leads to high adhesivity, highly efficient thickening and network building in suspension (Fig. 1e), and the ability to form materials and coatings with high surface area (Fig. 1f,g).

The formation of the branched structure is controlled by multiple factors, which include the hydrodynamics of shear, the initial polymer concentration in the injected solution and the rates of solvent–non-solvent mixing and polymer precipitation. We found that the key factor for formation of dendritic structures is the turbulent flow. Polymer solutions precipitated under laminar non-solvent flow yield nanofibres as described in our earlier report[18]. However, when the non-solvent medium was turbulently sheared, the precipitated structures were dendritic particles with colloid-scale features (Fig. 1a,b). To establish the correlation between flow regime and precipitated polymer structure, we investigated the outcome using a Couette cell with coaxially aligned cylinders. A solution of 5 wt% polystyrene (PS) in tetrahydrofuran (THF) was injected into a non-solvent medium sheared at various rates. The drastic change in the resulting polymer morphologies is illustrated in Supplementary Fig. 2. We observed a transition from spheroidal particles at low Re numbers to nanofibres in laminar flow. Branched fibres were precipitated at the highest shear possible in the Couette flow device where the flow became turbulent (Re ≈ 10,000). The high turbulence achieved in the rotor–stator IKA Magic Lab device (estimated Re > 100,000) results in the formation of well-developed hierarchical dendricolloids (Fig. 1b) with branches of micrometre-scale length and nanoscale diameter (Fig. 1c,d). We hypothesize that the hierarchically self-similar structure of the dendricolloids is templated by the multiscale fluid eddies in turbulent flow, which have a stochastic fractal organization[20]. This suggests a rather unexpected correlation between the dynamic turbulent flow structure and the morphology of the material precipitated in this otherwise highly disruptive environment.

We next correlated the structure of PS dendricolloids formed to the rate of polymer precipitation and molecular weight. Similar to our earlier reports[1,18], solutions of polymers with insufficient molecular entanglement precipitated into fragmented rod-like structures (Supplementary Fig. 3). The rate of polymer precipitation was varied by changing the polymer concentration and the chemical composition of the solvent–non-solvent mixture. The diverse structural outcomes are summarized in Fig. 2a. Dendritic nanofibrils resulted when PS was dissolved in THF at a concentration of 5–10 wt%. Within the same concentration range, PS solutions in *N*,*N*-dimethylformamide (DMF), dimethylacetamide (DMAc) or 1,4-dioxane formed sheet-like particles. Small shapeless 'chunks' precipitated at lower concentrations, regardless of the solvent. These results can be correlated to the rate of polymer precipitation during non-solvent infusion. Polymer phases are separated when the solution compositions cross the binodal phase-separation lines in the three-phase diagram, which are plotted in Fig. 2b. DMF, DMAc, and 1,4-dioxane show faster polymer phase separation. This is evident in the observed higher binodal curves with smaller one-phase regions compared to those of THF and is correlated with the lower solvent–non-solvent interaction parameter χ (Supplementary Fig. 4), which is used to qualitatively order the polymers in Fig. 2a. The

[1]Department of Chemical and Biomolecular Engineering, North Carolina State University, Raleigh, NC, USA. [2]Physical Chemistry and Soft Matter, Wageningen University, Wageningen, the Netherlands. [3]Department of Mechanical Engineering, University College London, London, UK. [4]Unilever Research and Development, Vlaardingen, the Netherlands. *e-mail: odvelev@ncsu.edu

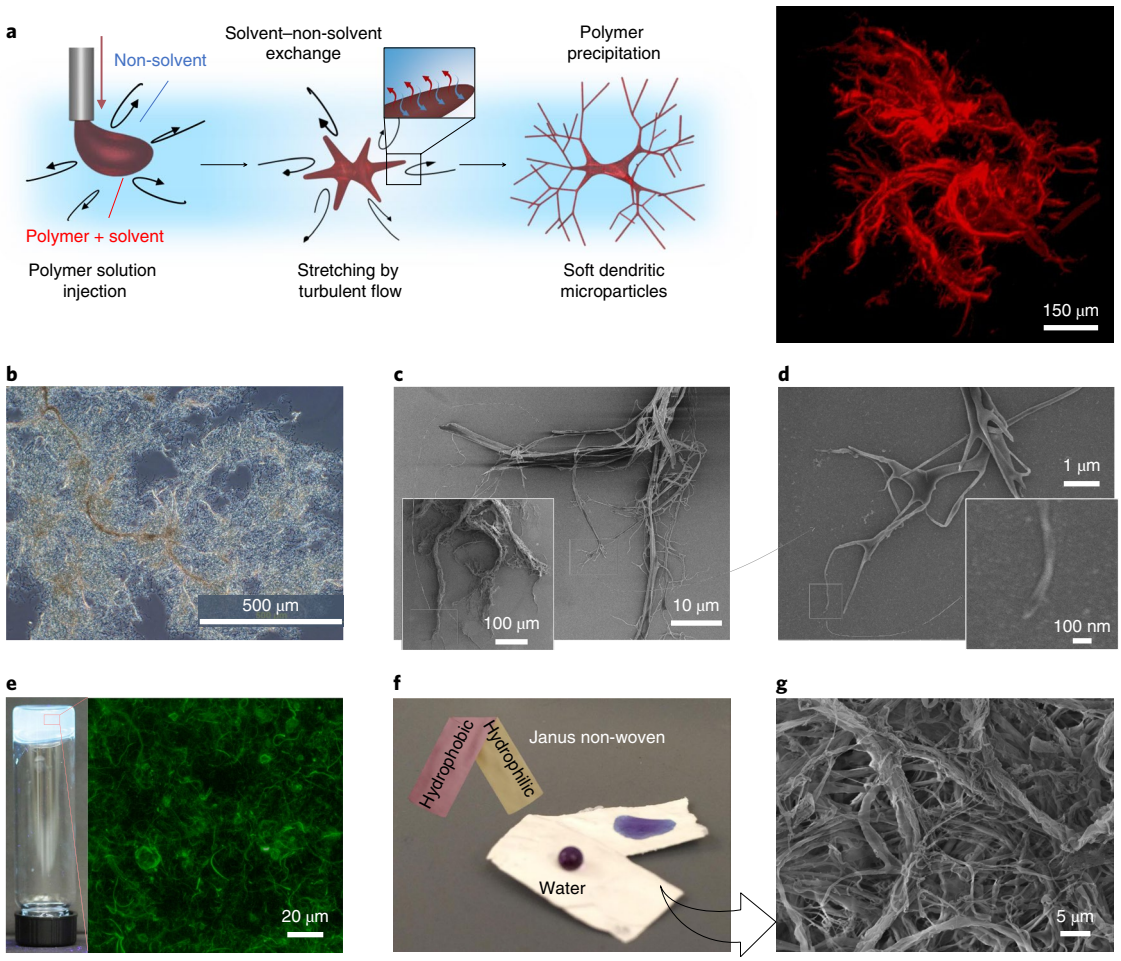

Fig. 1 | Fabrication and properties of soft dendritic colloidal microparticles. a, Schematic of the process leading to soft dendricolloid formation. Polymer solution is injected into a turbulently sheared non-solvent medium. It is randomly stretched by turbulent eddies and the polymer is precipitated into a branched structure. The image on the right is a confocal microscopy reconstruction of a PS dendricolloid particle. **b**–**d**, An optical microscopy (**b**) and SEM images (**c**,**d**) of PS dendricolloids. The colloids are hierarchically branched and surrounded by a nanofibre corona. **e**, A vial containing a gel of 0.5 vol% of CA soft dendritic microparticles in polyethylene glycol and a confocal microscopy image of its structure. The fibrils were labelled with fluorescein isothiocyanate. **f**, A photograph of a 'Janus' non-woven sheet composed of dried dendritic fibrillar layers of PS (superhydrophobic) and PVOH (superhydrophilic). **g**, SEM image of the PS layer surface morphology.

polymer precipitates rapidly from DMF, DMAc and 1,4-dioxane solutions, forming thin skins around the droplets, which are subsequently peeled off by the turbulent flow to yield two-dimensional sheets (Fig. 2a,c). On the other hand, the delayed precipitation of PS in THF/water leads to the formation of dendritic structures.

The branched nanofibre corona surrounding the soft colloids leads to remarkable adhesive properties. We evaluated their adhesion strength through lap shear strength testing. The specimens were prepared by drying 250 µl of a 1 wt% cellulose acetate (CA) dendricolloid suspension in ethanol in the gap between two glass slides (overlap area of $25 \times 13\,mm^2$). A typical tensile lap shear curve of these specimens is shown in Fig. 3a. The lap shear force of the CA dendricolloids on the glass substrate was as high as 425 N (1.3 MPa). This is a remarkable strength for such a small amount of dried particulate adhesive (~2 mg); for example, this tensile stress was larger than that of commercial two-sided Scotch tape (~1.04 MPa) as shown in Fig. 3b. Dendricolloids composed of other polymers also exhibited commensurate lap shear strengths; for example, polyvinylidene fluoride and polyvinyl alcohol exhibited lap shear strengths of ~107.2 N and 870.9 N, respectively (Supplementary Fig. 5).

Examination of the gap between the bound slides by scanning electron microscopy (SEM) shows that the soft nanofibre coronas create a multitude of contact points to the glass as illustrated in the inset of Fig. 3a. This implies that the strong adhesion observed in the shear tests is a result of contact splitting mechanism analogous to the previously investigated nanofibrous pads on gecko feet[12,16,21–23]. We further elucidated the physical origins of the adhesion, which could originate from capillary bridging of miniscule water menisci[24] or omnipresent van der Waals forces[12,13]. The role of the capillary bridging forces can be evaluated by a comparison of the adhesion strength to substrates of different hydrophobicity. Capillary force depends strongly on the water contact angle of the substrate and adherent material[13,25]. On hydrophobization, the contact angle of water on the slides changed from 25.3° to 77.4°, which would result in a twofold decrease in the capillary binding force (Supplementary Fig. 6 and equation (9) in Methods). However, we found that the adhesion strength of dendricolloids between the hydrophobized slides was similar to that between pristine glass (Fig. 3c). Thus, we conclude that the strong dendricolloid adhesion is not a result of capillary forces.

The alternative hypothesis is that the strong adhesion is a result of van der Waals attraction of the nanofibrils to the substrate. We evaluated the effect of these universal forces by measuring the lap shear strength of adhesive patches of dendricolloids infused

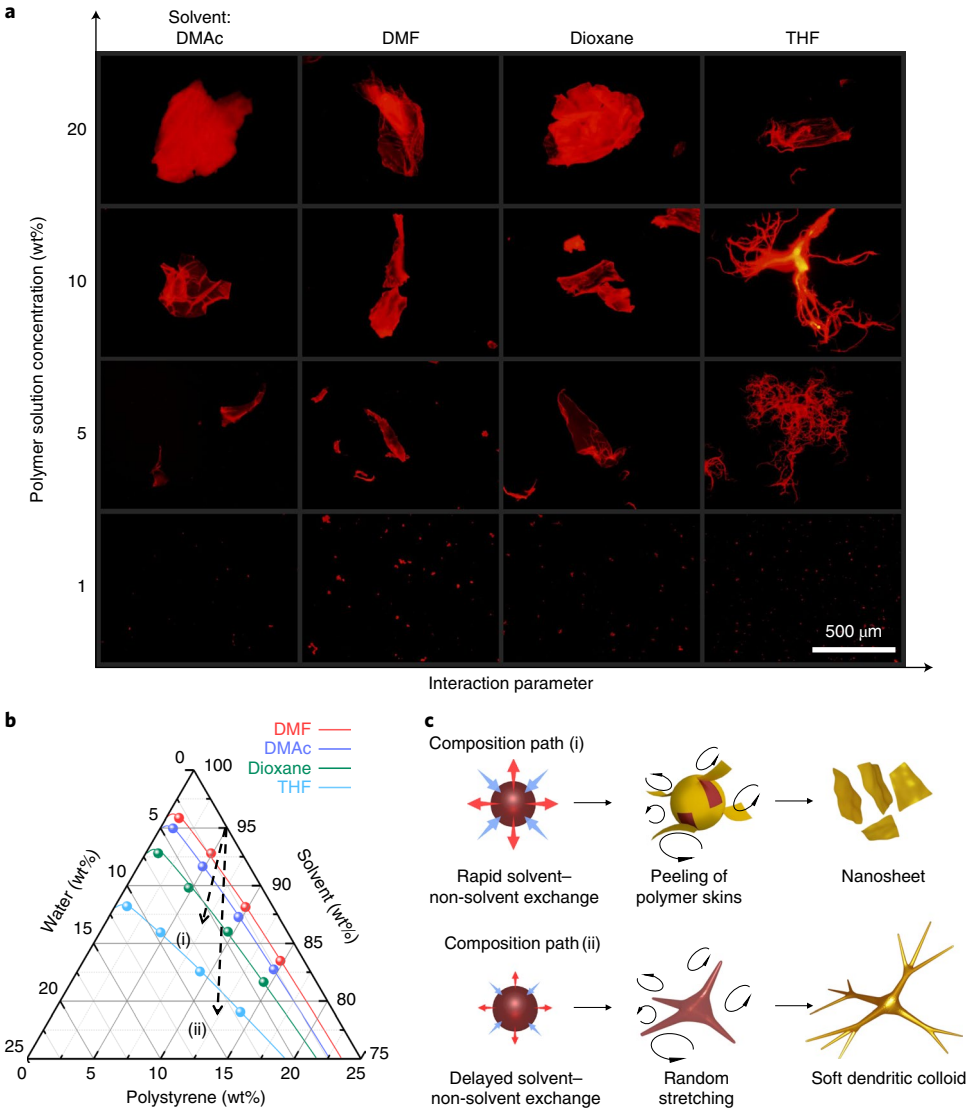

Fig. 2 | Conditions for dendricolloid formation. a, Fluorescence microscopy images of PS particulates (labelled with Nile red) precipitated in turbulently sheared water medium at different solvent–non-solvent pairings and solution concentrations. Sheet-like particles were precipitated from solvents with high affinity to water (DMF, DMSO and 1,4-dioxane). When PS was dissolved in THF, dendritic polymer structures were formed at a certain concentration range (5–10 wt%). **b**, The ternary phase diagram of PS, water (non-solvent) and solvents. Our hypothesis is that the phase trajectory of precipitation determines the morphological outcome. The hypothesized composition paths after injection demonstrate rapid precipitation for the DMF–water system (i) and delayed precipitation for the THF–water system (ii). **c**, Schematic of the mechanism of sheet-like and soft dendritic colloid formation depending on the composition paths shown in **b**. Rapid precipitation results in sheet-like particulates, while delayed precipitation leads to the formation of dendricolloids.

with organic liquids. According to Lifshitz theory, the van der Waals interaction depends strongly on the refractive index (RI) difference between the adhesive material and the surrounding medium[25]. The lap shear strength of CA dendricolloid binding will be minimized when the RI of the infused liquid medium matches that of CA. The media included polyethylene glycol (PEG 400) and diiodomethane, the RIs of which are ~1.466 (matching the CA RI of 1.47), and ~1.74, respectively. While there was a twofold decrease in lap shear strength with diiodomethane, the lap shear strength of both pristine and hydrophobized glass reached a deep minimum when the infused liquid matched the RI of the CA dendricolloids (Fig. 3c). Data on failure modes of the adhesive patches also show that they detach from the surfaces only in RI-matched media (Supplementary Fig. 7). This proves that the dendricolloid adhesion is predominantly driven by van der Waals forces, which has been established as the basis of the 'gecko leg' effect[12,13]. We further compared the adhesion force of CA dendricolloids and nanoparticles (Fig. 3d) whose surface areas were nearly the same at 21.03 $m^2 g^{-1}$ and 31.8 $m^2 g^{-1}$, respectively. The lap shear strength of the dendricolloid layer is 11.4 times larger than the nanoparticle layer of equal volume, indicating the dendritic structure enables much stronger physical adhesion. An evaluation of the adhesion force utilizing the Johnson–Kendall–Roberts adhesion model[26] also predicts an approximately eightfold increase with dendricolloids compared to spherical particles (equations (10)–(12)) in Methods). The high adhesion and hierarchical surface of the dried dendritic polymer particles also allows for simple deposition of superhydrophobic and superhydrophilic coatings (previously achievable by carbon-nanotube deposition[27]), as well as the formation of non-woven 'Janus' sheets with remarkable wetting properties, as shown in Fig. 1f and discussed in more detail in the Supplementary Information, including in Supplementary Figs. 8 and 9.

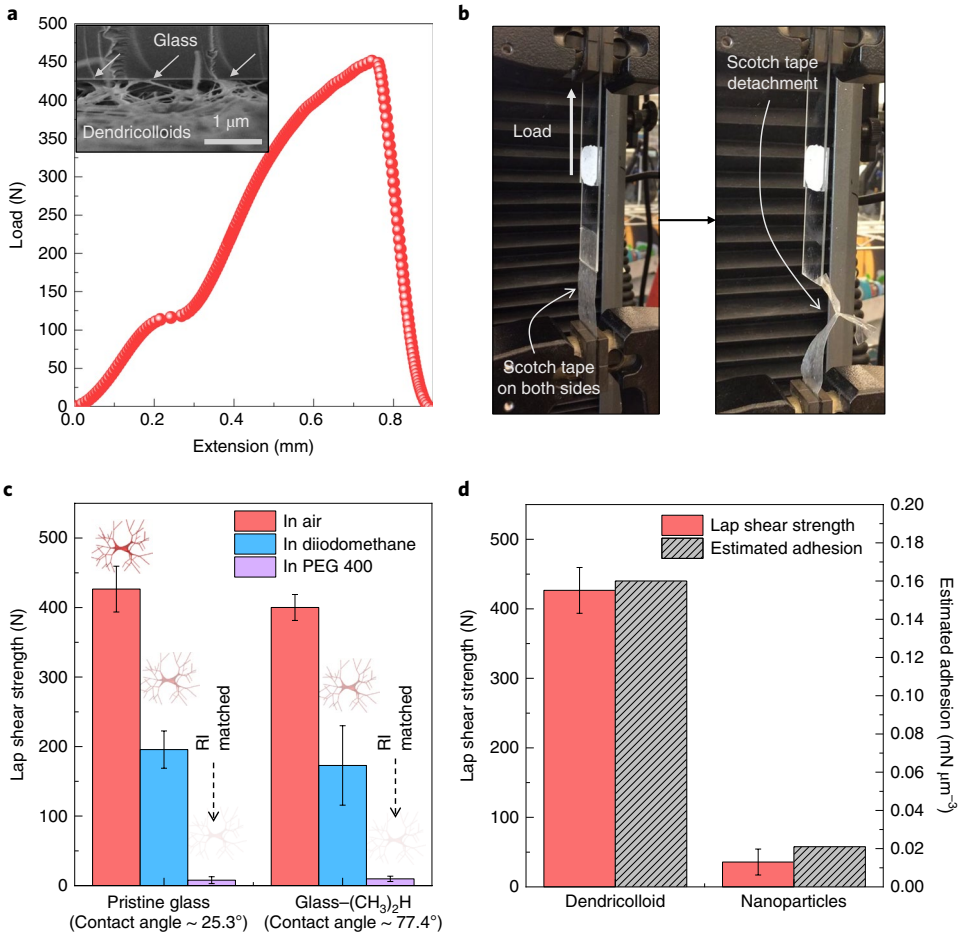

Fig. 3 | Adhesion characteristics of soft dendritic colloidal microparticles. a, Lap shear strength curve of CA dendricolloid layer between glass slides. The inset shows a magnified cross-section of the dendritic fibre patch. **b**, Example of the efficiency of these particles as dried adhesives between glass slides bound by 2 mg of CA dendricolloids in the white patch above and by two-sided Scotch tape below. The Scotch tape adhesive fails before the dendricolloid network. **c**, Maximum lap shear strength of CA dendricolloids deposited between pristine and hydrophobized glass substrates within air (red column, largest RI difference, $|n_{12} - n_{32}| = 1.16$), diiodomethane (blue column, moderate RI difference, $|n_{12} - n_{32}| = 0.87$) and PEG 400 (purple column, RI-matched solution, $|n_{12} - n_{32}| = 0.01$). These results prove the major role of the van der Waals forces in the adhesion. **d**, Lap shear strengths of equal amounts of CA nanoparticles and dendricolloids between two glass slides (red bars), compared to a simple adhesion model. Error bars indicate s.d. for three measurements at each point.

The soft dendritic microparticles proved to be highly effective thickening and gelation agents within liquid media. For example, as little as 0.5 vol% CA dendricolloids lead to gelation of polyethylene glycol (PEG 200) by forming a voluminous fibrillar network as shown in Fig. 1e. The efficiency of dendricolloids as rheological modifiers was evaluated via the dependence of storage modulus (G') on the volume fraction of suspensions in mineral oil (Fig. 4a and Supplementary Fig. 10). All samples exhibited gel-like properties in the linear viscoelastic regime with $G' \gg G''$ independent of frequency (ω). To confirm the role of fractal morphology on suspension rheology, we compared the G' and G'' of 1 w/v% suspensions of CA dendricolloids and CA nanoparticles in ethylene glycol (Fig. 4b). The dendricolloid suspension exhibited gel-like behaviour, with $G' \gg G''$ and both moduli being 3–4 log larger than those of fluid-like nanoparticle suspensions. Notably, after all suspensions in ethylene glycol were heated to 180 °C for 20 min causing the dissolution of the CA particles, the G' and G'' of all CA solutions collapse into a nearly identical curve (Supplementary Fig. 11).

Finally, the gelation efficiency of the soft dendritic particles was compared to fumed silica, one of the most common 'hard' dendritic colloids used as a commercial rheology modifier. The G' of mineral oil suspensions composed of CA dendricolloids and fumed silica are shown in Fig. 4c. The hydrophilic fumed silica forms fractal aggregates and a three-dimensional network structure in hydrophobic liquid such as mineral oil[5]. Both fumed silica and CA dendricolloid suspensions exhibited gel-like behaviour ($G' \gg G''$ and $G' \neq G'(\omega)$); however, at each volume fraction the G' of the CA dendricolloid suspension was larger than the fumed silica suspension. The higher gelation efficiency of the dendricolloids is probably a result of the formation of a three-dimensional network of cohesive soft fibrils. We investigated the contribution of van der Waals interactions to the dendricolloids' rheology characteristics by again utilizing the RI-matching technique. CA dendricolloids were suspended in ethylene glycol, PEG 200 and PEG 400. The transition to nearly transparent RI-matched suspension in PEG 400 correlated to a change from highly elastic, gel-like behaviour to weakly elastic, fluid-like behaviour (Fig. 4d and Supplementary Fig. 12). Given the strong dependence of the G' and G'' of the suspensions on the RI difference (Fig. 4d)[25], we conclude again that the van der Waals forces play a major role in the strong network-building ability of the soft dendritic particles. The joint action of large excluded volume and nanofibrillar contact splitting adhesion dramatically increases the gelation ability of the dendricolloids in comparison to conventional particle

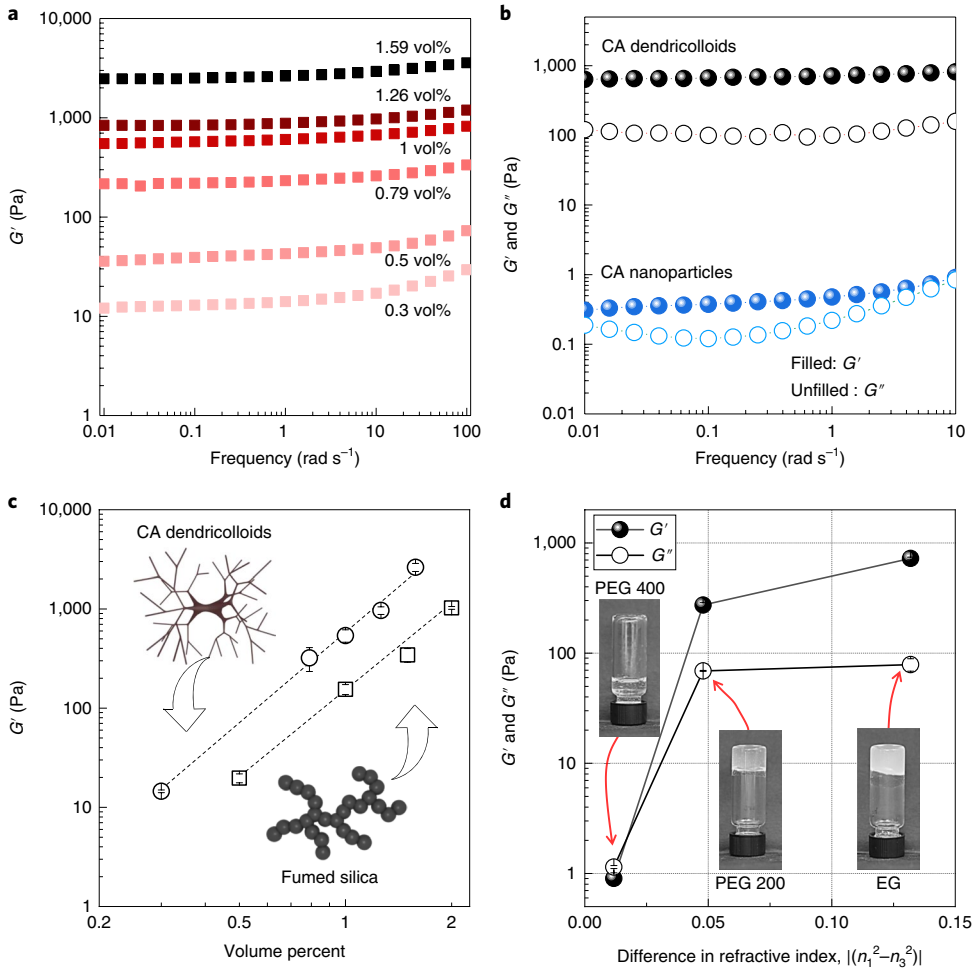

Fig. 4 | Structuring capability of soft dendricolloids in liquid suspensions. a, Storage modulus (G') versus frequency of CA dendricolloids suspensions in mineral oil with varying volume fractions. **b**, Magnitude of the G' and G'' of 1 w/v% of CA dendricolloids (black) and CA nanospheres (blue) in ethylene glycol. The dendritic morphology leads to a three- to four-order increase of the magnitude of both moduli. **c**, Dependence of the storage modulus (G') on the volume % of CA dendricolloids (circles) and fumed silica (squares) in mineral oil at a frequency of 1 rad s^{-1}. At any volume fraction, the CA dendricolloids have higher efficiency in increasing the storage modulus of mineral oil. **d**, The change in storage modulus (G', filled) and loss modulus (G'', unfilled) of 1 w/v% of CA dendricolloid versus the difference between the RIs of the polymer and PEG media (related to the van der Waals force) at 1 rad s^{-1}. Error bars indicate s.d. for three or four measurements at each point. A dramatic decrease in the shear moduli was observed as the RI difference decreases.

gelators. As this gelation effect relies on omnipresent van der Waals forces, it is rather universal, which was illustrated by preparing gels containing 1 vol% of CA dendricolloids in numerous common liquids (Supplementary Fig. 13). This strong structuring capability could also be used to prepare aerogels by freeze drying (Supplementary Fig. 14).

In summary, we present here a class of soft matter with a dendritic morphology and exceptional adhesion and structuring properties. The dendricolloids are orders of magnitude larger than the molecular polymer dendrimers that have been of large interest before[28–30]. Thus, they fill a previously little explored size domain of fractal soft matter. Their nanofibre coronas lead to strong adhesion to almost any surface because of van der Waals attraction. This strong adhesion was shown to be similar in physical origin to the unusual sticking of the legs of gecko lizards. However, the properties of this class of materials are also likely to be strongly dependent on the intertwining of nanofibrils, the degree of branching, the large excluded volume and the stress distribution along the fractal backbone. Thus, they could present a fascinating system for further fundamental studies. Moreover, the strong adhesion and structuring capability of this unusual class of colloids could enable numerous applications, such as components of next-generation functional coatings, non-wovens, filtration membranes, cell scaffolds, soft composite materials and functional constituents of consumer goods and pharmaceutical products.

Online content

Any methods, additional references, Nature Research reporting summaries, source data, extended data, supplementary information, acknowledgements, peer review information; details of author contributions and competing interests; and statements of data and code availability are available at https://doi.org/10.1038/s41563-019-0508-z.

Received: 15 December 2018; Accepted: 13 September 2019;
Published online: 14 October 2019

References

1. Alargova, R. G., Bhatt, K. H., Paunov, V. N. & Velev, O. D. Scalable synthesis of a new class of polymer microrods by a liquid–liquid dispersion technique. *Adv. Mater.* **16**, 1653–1657 (2004).
2. Bahng, J. H. et al. Anomalous dispersions of 'hedgehog' particles. *Nature* **517**, 596–599 (2015).

3. Zhu, J. Brached aramid nanofibers. *Angew. Chem. Int. Ed.* **56**, 11744–11748 (2017).
4. Pääkkö, M. et al. Enzymatic hydrolysis combined with mechanical shearing and high-pressure homogenization for nanoscale cellulose fibrils and strong gels. *Biomacromolecules* **8**, 1934–1941 (2007).
5. Khan, S. A. & Zoeller, N. J. Dynamic rheological behavior of flocculated fumed silica suspensions. *J. Rheol.* **37**, 1225–1235 (1993).
6. Koos, E. & Willenbacher, N. Capillary forces in suspension rheology. *Science* **331**, 897–900 (2011).
7. Cadirov, N., Booth, J. A., Turner, K. L. & Israelachvili, J. N. Influence of humidity on grip and release adhesion mechanisms for gecko-inspired microfibrillar surfaces. *ACS Appl. Mater. Interfaces* **9**, 14497–14505 (2017).
8. King, D. R., Bartlett, M. D., Gilman, C. A., Irschick, D. J. & Crosby, A. J. Creating gecko-like adhesives for 'real world' surfaces. *Adv. Mater.* **26**, 4345–4351 (2014).
9. Ge, L., Sethi, S., Ci, L., Ajayan, P. M. & Dhinojwala, A. Carbon nanotube-based synthetic gecko tapes. *Proc. Natl Acad. Sci. USA* **104**, 10792–10795 (2007).
10. Kwak, M. K., Jeong, H. E. & Suh, K. Y. Rational design and enhanced biocompatibility of a dry adhesive medical skin patch. *Adv. Mater.* **23**, 3949–3953 (2011).
11. Qu, L., Dai, L., Stone, M., Xia, Z. & Wang, Z. L. Carbon nanotube arrays with strong shear binding-on and easy normal lifting-off. *Science* **322**, 238–243 (2008).
12. Autumn, K. et al. Adhesive force of a single gecko foot-hair. *Nature* **405**, 681–685 (2000).
13. Autumn, K. et al. Evidence for van der Waals adhesion in gecko setae. *Proc. Natl Acad. Sci. USA* **99**, 12252–12256 (2002).
14. Tian, Y. et al. Adhesion and friction in gecko toe attachment and detachment. *Proc. Natl Acad. Sci. USA* **103**, 19320–19325 (2006).
15. Sahni, V., Harris, J., Blackledge, T. A. & Dhinojwala, A. Cobweb-weaving spiders produce different attachment discs for locomotion and prey capture. *Nat. Commun.* **3**, 1106 (2012).
16. Kamperman, M., Kroner, E., Del Campo, A., McMeeking, R. M. & Arzt, E. Functional adhesive surfaces with 'Gecko' effect: the concept of contact splitting. *Adv. Eng. Mater.* **12**, 335–348 (2010).
17. Hawthorn, A. C. & Opell, B. D. van der waals and hygroscopic forces of adhesion generated by spider capture threads. *J. Exp. Biol.* **206**, 3905–3911 (2003).
18. Smoukov, S. K. et al. Scalable liquid shear-driven fabrication of polymer nanofibers. *Adv. Mater.* **27**, 2642–2647 (2015).
19. Haase, M. F., Stebe, K. J. & Lee, D. Continuous fabrication of hierarchical and asymmetric bijel microparticles, fibers, and membranes by solvent transfer-induced phase separation (STRIPS). *Adv. Mater.* **27**, 7065–7071 (2015).
20. Procaccia, I. Fractal structures in turbulence. *J. Stat. Phys.* **36**, 649–663 (1984).
21. Bhushan, B. Adhesion of multi-level hierarchical attachment systems in gecko feet. *J. Adhes. Sci. Technol.* **21**, 1213–1258 (2007).
22. Arzt, E., Gorb, S. & Spolenak, R. From micro to nano contacts in biological attachment devices. *Proc. Natl Acad. Sci. USA* **100**, 10603–10606 (2003).
23. Raut, H. K. et al. Gecko-inspired dry adhesive based on micro-nanoscale hierarchical arrays for application in climbing devices. *ACS Appl. Mater. Interfaces* **10**, 1288–1296 (2018).
24. Huber, G. et al. Evidence for capillarity contributions to gecko adhesion from single spatula nanomechanical measurements. *Proc. Natl Acad. Sci. USA* **102**, 16293–16296 (2005).
25. Israelachvili, J. N. *Intermolecular and Surface Forces* (Elsevier, 2011).
26. Johnson, K. L., Kendall, K. & Roberts, A. D. Surface energy and the contact of elastic solids. *Proc. R. Soc. A* **324**, 301–313 (1971).
27. Lau, K. K. S. et al. Superhydrophobic carbon nanotube forests. *Nano Lett.* **3**, 1701–1705 (2003).
28. Buhleier, E., Wehner, W. & Vögtle, F. 'Cascade'- and 'nonskid-chain-like' syntheses of molecular cavity topologies. *Synthesis* **1978**, 155–158 (1978).
29. Hawker, C. J. & Fréchet, J. M. J. Preparation of polymers with controlled molecular architecture. a new convergent approach to dendritic macromolecules. *J. Am. Chem. Soc.* **112**, 7638–7647 (1990).
30. Astruc, D., Boisselier, E. & Ornelas, C. Dendrimers designed for functions: from physical, photophysical, and supramolecular properties to applications in sensing, catalysis, molecular electronics, photonics, and nanomedicine. *Chem. Rev.* **110**, 1857–1959 (2010).

Acknowledgements

This study was supported by grants from US National Science Foundation, no. CMMI-1825476 and partially no. CBET-1604116. We also thank NC State University for support through 2017 Chancellors Innovation Fund Award and Unilever Research. We thank L. Hsiao, S. Khan and M. Dickey for discussions and generously providing their rheometer, goniometer and mechanical testing machine facilities. We thank the Cellular and Molecular Imaging Facility at NC State University for their help with confocal imaging supported by the National Science Foundation (grant no. DBI-1624613).

Author contributions

The initial discovery of the dendricolloid formation was made by S.R. and O.D.V. The experimental design and data analysis were done by O.D.V., S.R., A.H.W., R.S.B. and S.D.S. The experimental laboratory work on dendricolloid synthesis and characterization was performed by S.R., A.H.W., and R.S.B. S.R. and O.D.V. were primary writers of the manuscript, and O.D.V. was the principal investigator. All authors discussed the results and provided feedback on the manuscript.

Competing interests

S.R. and O.D.V. are inventors on a patent application submitted by NC State University, which covers synthesis and properties of fractal polymer colloids.

Additional information

Supplementary information is available for this paper at https://doi.org/10.1038/s41563-019-0508-z.

Correspondence and requests for materials should be addressed to O.D.V.

Reprints and permissions information is available at www.nature.com/reprints.

Publisher's note Springer Nature remains neutral with regard to jurisdictional claims in published maps and institutional affiliations.

Methods

Fabrication of soft dendritic microparticles. We demonstrate dendricolloids composed of PS (weight-averaged molecular mass $M_w = 230{,}000$ Da, Sigma-Aldrich), CA (number averaged molecular mass $M_n = 30{,}000$ Da, Sigma-Aldrich), polyvinyl alcohol (PVOH, Mowiol 18–88, 86.7–88.7% hydrolysis, $M_w = 130{,}000$ Da, Sigma-Aldrich) and polyvinylidene fluoride (PVDF, $M_w = 530{,}000$ Da, Sigma-Aldrich). The polymer solution concentrations, solvents and non-solvents for fabricating the dendricolloids of the listed polymers are listed in Supplementary Table 1.

The polymer–solvent mixture was directly injected into the shear zone of the IKA Magic Lab device (IKA Works Inc.) operating at 20,000 r.p.m. (Supplementary Fig. 1). The PVOH dendricolloids were crosslinked with glutaraldehyde in acetone. All samples were washed with water and stored as ethanol or water suspensions. Couette flow experiments were performed by shearing a medium in a concentric rotating cylinder device with a larger tube (internal diameter, 14.5 mm) and inner coaxial 9.5 mm stainless steel rod rotated by a Servodyne (150–6,000 r.p.m.) mixer.

Characterization of the soft dendricolloid morphology. The morphologies of the soft dendritic colloidal particles were visualized through a confocal microscope, fluorescence microscope (BX-61 Olympus) and field emission scanning electron microscope (FEI Verios 460L scanning electron microscope). For fluorescence visualization, the PS dendricolloids were labelled with Nile red while CA dendricolloids were labelled with fluorescein isothiocyanate (Fig. 1e). The images in Fig. 2a were processed with ImageJ to adjust brightness and contrast. The adjustment was applied equally across the all of the images. In preparing the dendricolloids shown in Fig. 1a,c,d, 4 wt% PS in THF solution was injected into a water non-solvent and sheared within the IKA Magic Lab device at 20,000 r.p.m. The PS dendritic samples were collected and diluted in isopropyl alcohol and, to ensure minimum particle entanglement, were vortexed and sonicated before field emission scanning electron microscope and confocal imaging. For confocal imaging, the PS dendricolloids were further diluted in a 65 wt% zirconia nanoparticles (PCPN, Pixelligent) in ethylene glycol solution to match the refractive indices of PS and the medium. The dendricolloids were imaged with a Zeiss LSM 880 confocal microscope and z-stacks were taken at 1,024 × 1,024 x–y resolution. Post-imaging analysis and animation were created using Imaris and Zen software.

Lap shear testing. The lap shear strength of the soft dendricolloids was measured using a common testing machine (Instron 5943). The crosshead speed of the testing device was 5.0 in min^{-1}. First, 250 µl of a 1 wt% suspension of CA, PVDF or PVOH dendricolloids in ethanol was deposited between two glass slides (overlapping area, 25 × 13 mm^2) and left to dry at 60 °C for 24 h. Every set of lap shear strength data was averaged from three specimens. We also measured the lap shear strength of the CA dendricolloids between two glass slides after infusing the dried dendricolloid patch with diiodomethane (Sigma-Aldrich) and polyethylene glycol (Sigma-Aldrich, $M_n = 400$ Da). To investigate the contribution of capillary forces, we measured lap shear strength on both pristine and hydrophobized glass slides. Hydrophobization of the glass slides was completed by first cleaning the slides with NOCHROMIX solution to form hydroxyl groups on the surface. The cleaned and dried glasses were then immersed in a 0.01 wt% chlorodimethylsilane in toluene mixture for 2 h. To remove unreacted substances, we used 100 ml of toluene, isopropyl alcohol, acetone and water under sonication. After cleaning, the hydrophobized glass slides were placed in a vacuum oven (105 °C) for 24 h.

Porous non-woven fabrication. To create a non-woven (paper-like) material, 10 ml of 0.5 wt% dendricolloid in ethanol suspension was deposited on a polytetrafluoroethylene (PTFE) sheet (McMaster). The PTFE sheet with dendricolloid suspension was then placed in an oven (65 °C) to dry. After drying, the dendricolloids form a non-woven sheet that is easily removed from the PTFE surface.

Janus non-woven fabrication. First, 10 ml of 1 wt% PVOH and PS dendricolloid suspensions in ethanol were prepared. The PS dendricolloid suspension was then deposited on a cellulose pad followed by the PVOH suspension. The PS and PVOH dendricolloids on the pad were vacuum-filtered and the layered material was deposited between Teflon sheets. The dendricolloids were dried in an oven (65 °C) and the dried non-woven was carefully peeled off.

Rheology characterization of dendricolloid suspensions. The viscoelastic properties of the soft dendritic colloid suspensions were evaluated with a rheometer (Discovery HR-2, TA Instruments) equipped with a sand-blasted plate and plate geometry (40 mm diameter and 1 mm gap size). The suspensions were pre-sheared at 1 s^{-1} for 10 s followed by 5 min equilibration. For the small amplitude measurements, we fixed strain within the linear viscoelastic region. To prepare the CA dendricolloids in mineral oil (Sigma-Aldrich) suspension, the ethanol in CA dendricolloid suspension was replaced with hexane by centrifugation. Mineral oil was added into the CA dendricolloid in hexane suspensions and then the hexane was removed from the suspension by evaporation at 65 °C for 24 h. The CA dendricolloid–mineral oil suspension was then homogenized with a magnetic stirrer (100 r.p.m.) for 12 h before measuring the viscoelastic properties. The hydrophilic fumed silica used in the comparative experiments was purchased from Sigma-Aldrich.

Estimation of capillary force between dendricolloids and glass. To evaluate the origin of the dendricolloid adhesion, we measured the lap shear strength on both pristine glass and a hydrophobized glass. Assuming that the volume of water comprising the capillary bridges between the dendricolloids and the glass is constant, we compared the capillary forces on both types of glass surfaces. As the dendricolloids can be approximately described as consisting of a multitude of nanofibres, we approximated their structure with cylinders of equivalent surface area (Supplementary Fig. 6). The average radius of the fibres was obtained from the Brunauer–Emmett–Teller surface area (21.03 m^2 g^{-1}). From the surface area, the average radius can be calculated following the equation

$$R_1 = \frac{2}{S\rho} \tag{1}$$

where S is the surface area per unit mass and ρ is the density of CA (1.3 g cm^{-3}). From equation (1), the average radius (R_1) of the dendricolloids is 73.2 nm. Assuming the length of the dendricolloid fibre (L) is much bigger than the transversal contact length s,

$$L + s \cong L \tag{2}$$

The Young–Laplace equation for capillary pressure is given by

$$\Delta P = \gamma_w \left(-\frac{1}{r_1} + \frac{1}{r_2} \right) \tag{3}$$

where γ_w is surface tension of water (72.1 mN m^{-1}) and r_1 and r_2 are the radii of curvature of the water meniscus formed between a cylinder and a flat substrate. Here, we can assume $\left|\frac{1}{r_1}\right| \gg \left|\frac{1}{r_2}\right|$ due to the long cylindrical geometry,

$$\Delta P = \gamma_w \left(-\frac{1}{r_1} + \frac{1}{r_2} \right) \cong -\gamma_w \frac{1}{r_1} \tag{4}$$

The curvature of radii in such a water meniscus between a curved surface and a flat surface is given by[31]

$$r_1 = \frac{R_1(1 - \cos\beta) + D}{\cos(\theta_1 + \beta) + \cos\theta_2} \tag{5}$$

where D is the distance between the flat substrate and cylinder, θ_1 and θ_2 are contact angles between water and cylinder and between water and the substrate, respectively. β is the central angle of a circular sector consisting of three points: (1) a point where three phases (water, cylinder, and air) meet each other; (2) the centre of meniscus contacting the cylinder; and (3) the centre of the cylinder. A schematic illustrating these parameters is shown in Supplementary Fig. 6. By plugging equation (5) into equation (4),

$$\Delta P \cong -\frac{\gamma_w(\cos(\theta_1 + \beta) + \cos\theta_2)}{R_1(1 - \cos\beta) + D} \tag{6}$$

The total capillary force between cylinder and flat surface is given by

$$F = 2(L + 2s)\gamma_w - 2sL\Delta P \tag{7}$$

The total capillary force per unit length of the fibres is ($L + 2s \cong L$)

$$F/L = 2\gamma_w - 2s\Delta P \tag{8}$$

By plugging equation (6) into equation (8), the capillary force per unit length of the fibre is given by

$$F/L \cong 2\gamma_w \left(1 + \frac{s(\cos(\theta_1 + \beta) + \cos\theta_2)}{R_1(1 - \cos\beta) + D} \right) \tag{9}$$

where $s = R_1 \sin\beta - r_1[1 - \cos(\theta_1 + \beta)]$. The water contact angles on bare glass and hydrophobized glass are 25.3° and 77.4°, respectively (with that of CA being 53°). The numerically estimated capillary forces with pristine glass and hydrophobized glass substrates are shown in Supplementary Fig. 6 with the area of the water menisci.

Estimation of the adhesion strength of dendricolloids and nanoparticles. To compare the adhesive strength of different polymer dendricolloids, we calculated the force needed to pull off a nanofibre of equivalent diameter. The pull-off force of a spherical particle is given by[26]

$$F_{\text{sphere}} = -\frac{3}{2}\pi w R \tag{10}$$

where w is the work of adhesion (~100 mN m^{-1}) between the substrate and the particle and R is the particle radius. The modified Johnson–Kendall–Roberts model for cylindrical structure adhesion is expressed as[32,33]

$$F_{\text{cylinder}} = -\frac{3}{2}\left(\frac{\pi w^2 E^* R'}{2}\right)^{\frac{1}{3}} \quad (11)$$

where R' is the radius of cylinder and E^* is expressed in terms of Young's moduli of the particle and substrate as

$$E^* = \left[\frac{\left(1-\nu_1^2\right)}{E_1} + \frac{\left(1-\nu_2^2\right)}{E_2}\right]^{-1} \quad (12)$$

where E_i is the Elastic moduli of the particle (CA, 4.7 GPa) and substrate (glass, 70 GPa) and ν_i is Poisson's ratio of the particles (0.39) and the substrate (0.24).

Data availability

All data, experimental details and supplemental analysis are available in the main text or the supplementary material. Further related raw data images and files are available on request from the authors.

References

31. Butt, H. & Kappl, M. *Surface and Interfacial Forces*. (John Wiley & Sons, Weinheim, 2009).
32. Chaudhury, M. K., Weaver, T., Hui, C. Y. & Kramer, E. J. Adhesive contact of cylindrical lens and a flat sheet. *J. Appl. Phys.* **80**, 30–37 (1996).
33. Spolenak, R., Gorb, S., Gao, H. & Arzt, E. Effects of contact shape on the scaling of biological attachments. *Proc. R. Soc. A* **461**, 305–319 (2005).